Article:
Kern, LS, Hine, PJ and Gusev, AA (2019) Optimizing the damping properties of unidirectional composites by incorporating carbon fibers with a thin viscoelastic coating. Composite Structures, 208. pp. 879-890. ISSN 0263-8223

https://doi.org/10.1016/j.compstruct.2018.10.043

Optimizing the damping properties of unidirectional composites by incorporating carbon fibers with a thin viscoelastic coating

Leyla S.Kern[1], Peter J.Hine[2], and Andrei A.Gusev*[1]

1 - Institute of Polymers, Department of Materials, ETH Zürich, 8093 Zürich, Switzerland

2 - Soft Matter Group, School of Physics and Astronomy, University of Leeds, Leeds, LS2 9JT, UK

Abstract. Two distinct techniques were used to predict, and then optimize, the viscoelastic properties of unidirectional carbon fiber/epoxy composites where the carbon fibers were coated with a thin lossy coating. First, finite element models with hexagonal and random microstructures were used to predict the effect of various parameters on the five independent stiffness constants of such unidirectional composites, most importantly that of the ratio of the coating thickness to the fiber diameter. Second, these predictions were compared to those obtained from the n-layered micromechanical model of Hervé and Zaoui and it was shown that the modelling predictions were remarkably accurate. It was found that while the longitudinal moduli were little affected by the presence of the coating, both the transverse and shear moduli showed a maximum loss (and a significant enhancement compared to uncoated fibers) for a coating thickness ratio of 0.001 corresponding to a coating thickness of ~10nm for a typical industrial carbon fiber. The enhancement of the shear loss moduli was shown to be particularly important, as a study of the eigenfrequencies of a simply supported viscoelastic plate strip showed that the shear deformation mode was activated and hence led to a significant increase in the effective vibration damping.

Keywords: viscoelastic; composite materials; finite element; vibration damping; design.

*Corresponding author.

E-mail address: gusev@mat.ethz.ch (A.A. Gusev).

1 Introduction

Vibration damping is a relevant topic in various applications. Not only can vibrations cause structural instability but also trigger noise. Thus, improvement in vibration control is of standing interest for many industries. Composite materials are often favored to pure materials as they can be designed to provide several desired properties simultaneously while the properties are mutually exclusive in pure materials. Polymers are widely employed in composites due to their high dissipation and light weight. Combined with a stiff but non-lossy material, one can create composites that exhibit both, high stiffness and high dissipation [1, 2]. However, defining suitable properties of a composite to achieve optimal performance is a challenging task. It is thus of interest to make use of homogenization models to determine the effective properties of heterogeneous materials. Commonly used models were derived by Hashin, Hill, Christensen and later by Hervé and Zaoui [3-8].

In the last decades, many approaches were made on assessing the potential of micromechanical models and estimating the accuracy by comparison with results of numerical simulations and experimental measurements [9-11]. Recently, Gusev presented time-domain finite element simulation for composites with different microstructures, including composites with viscoelastic coated spherical inclusions. It was found that the n-layered model [8] is remarkably accurate even in the case of high stiffness contrast and thin coating layers [12-14]. Unwin et al. further highlighted the progress in damping techniques by the use of polymer composites with viscoelastic coated spherical inclusions [15, 16]. It was shown that experimental measurements were in close agreement with the analytic prediction.

Another work showed the agreement of numerical models and measurements for unidirectional glass/epoxy composites [17]. The prediction of elastic moduli of fiber-reinforced composites was addressed by the composite cylinder model of Hashin and Rosen [5, 18] and further approached by Christensen and Lo [4]. Moreover, viscoelastic composites can be studied using the viscoelastic correspondence principle and replacing the static moduli by complex

viscoelastic ones [19]. The elastic-viscoelastic correspondence principle has been discussed and used in a recent finite-volume unit cell homogenization study to relate the governing equations in the time and Laplace-Carson domains [20]. In our recent work, uncoated carbon fibers (and glass fibers) in a viscoelastic matrix were studied by comparison with frequency-domain finite element estimates [21].

In the present work, frequency-domain finite element simulations were further applied to determine the effective moduli of viscoelastic coated fiber-reinforced composites. The obtained estimates are then used to examine the accuracy of the model for multiply coated fiber-reinforced composites by Hervé and Zaoui [6] and compared with respect to the fiber coating thickness and the volume fractions of matrix and fibers. Moreover, examples of applications are presented where the previously derived moduli are used to determine complex eigenfrequencies of composite viscoelastic plate strips, when deformed in simple bending.

2 Theoretical simulations

2.1 Finite element model

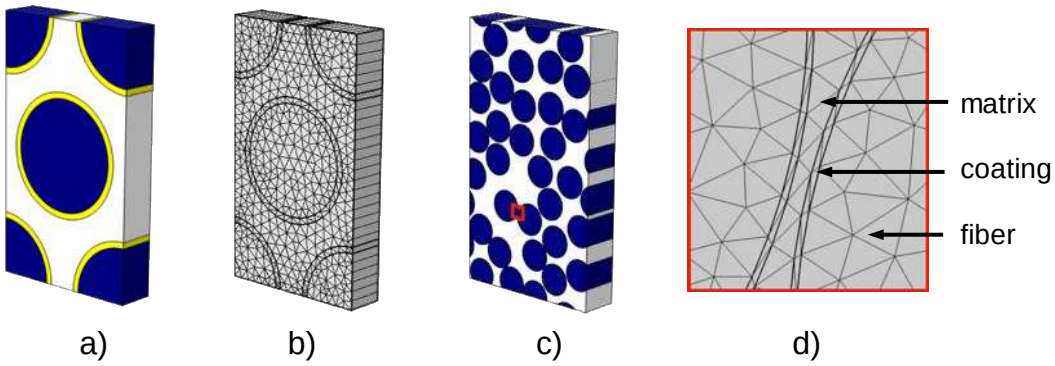

Figure 1: Periodic finite element model of coated fiber composites in hexagonal structure (a) and the corresponding mesh (b). A model with 32 random fibers is illustrated in Figure c and a magnified sketch of the mesh between two nearly touching fibers is shown in Figure d.

The effective viscoelastic moduli of unidirectional coated fiber reinforced composites were first estimated using finite element models. Two kinds of models were studied employing unit cells with either a regular hexagonal configuration of fibers (cf. Figure 1a) or randomly distributed fibers (cf. Figure 1c). The latter was generated using a Monte Carlo method by randomly dispersing 32 identical fibers. A detailed description of the Monte Carlo method and the homogenization procedure was given in our recent work [21].

The models were meshed with prismatic elements obtained by generating a two-dimensional triangular mesh first on one of the two faces orthogonal to the fibers. This mesh was then extruded to the opposite face of the unit cell, creating prismatic elements along the fibers as it is seen in Figure 1b. It is further shown in Figure 1d that in the case of random models, where fibers can come arbitrarily close, the mesh has smaller elements in the regions between two close fibers. Likewise, the mesh is finer within the coating layers.

Frequency-domain finite element simulations were performed using COMSOL Multiphysics (www.comsol.com) with MATLAB (www.matlab.com), as described in our recent work [21] where a frequency-domain homogenization procedure for the effective viscoelastic constants

was introduced and validated. The procedure is based on the elastic-viscoelastic correspondence principle and it allows one to obtain the effective viscoelastic constants of composite materials on the basis of their periodic computer models using the weighted residual Galerkin finite element method with complex viscoelastic moduli of the constituent phases. The multi-frontal direct sparse complex arithmetic MUMPS solver (mumps.enseeiht.fr) was used in all numerical calculations.

The models with 32 randomly dispersed fibers had up to two million degrees of freedom and took several minutes computing time. Calculations with hexagonal models, containing only two fibers, were accordingly faster.

2.2 Constituent properties

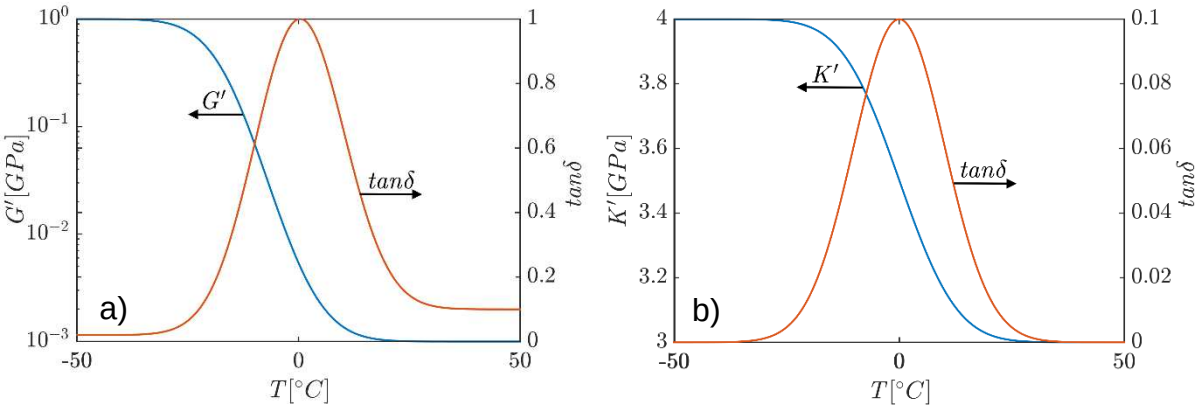

Figure 2: Temperature dependence of the shear modulus (a) and the bulk modulus (b) of the viscoelastic coating layer. The blue line corresponds to the storage moduli while the red line shows the loss factor tanδ.

Composites with coated carbon fibers are studied. Temperature-independent moduli were assumed for the fibers and the matrix, whereas the moduli of the viscoelastic coating layer varied as illustrated in Figure 2. The temperature dependence for the shear and the bulk modulus, given by $G = G'(1 + i\tan\delta)$ and $K = K'(1 + i\tan\delta)$, respectively, is shown.

From Figure 2a it is seen that the storage shear modulus G' (blue curve) changes from 1 GPa to 1 MPa across the glass transition temperature (T_g= 0°C), with the corresponding loss factor

$\tan\delta$ (red curve) reaching a maximal value of 1 at the glass transition temperature, T_g. The bulk modulus ranges from $K' = 4$ GPa to 3 GPa with a maximal $\tan\delta$ of 0.1, as shown in Figure 2b [13]. The assumed temperature-independent moduli of the matrix are G= (1+i0.02) GPa and K=4 GPa, which is equivalent to the moduli of the coating layer at T=-50°C. For carbon fibers, temperature-independent transversely isotropic properties are assumed with the moduli given in Table 1 [22]. Clearly, the stiffness is highest in the fiber direction.

E_{11}[GPa]	E_{22}[GPa]	G_{12}[GPa]	G_{23}[GPa]	υ_{12}
230	15	15	7	0.2

Table 1: The chosen constituent properties for the carbon fibers.

For the constituent phases, linear viscoelastic stress-strain relations are assumed at a frequency of 1 Hz ($\omega = 2\pi$)

$$\boldsymbol{\sigma}(\boldsymbol{t}) = \boldsymbol{C}(\omega)\boldsymbol{\varepsilon}e^{i\omega t} \tag{1}$$

where $\boldsymbol{\sigma}$ is the stress tensor, $\boldsymbol{\varepsilon}$ the strain amplitude tensor and $\boldsymbol{C}$ the complex viscoelastic moduli, respectively whereas ω and t denote the angular frequency and the time, respectively [19].

2.3 Micromechanics model

A micromechanical model to predict the effective moduli of n-layered composites was derived by Hervé and Zaoui for fiber-reinforced composites with multiple layers of coated fibers [6]. The layers are represented by shells covering an inner core as illustrated in
Figure 3. The elastic strain and stress fields are determined for the n-layered composite cylinder embedded in an infinite matrix and subjected to uniform loading conditions at infinity.
As perfect bonding at the interfaces is assumed, the continuity conditions of the stress and displacement fields must hold, and they are written as

$$\boldsymbol{J}_k(R_k)\boldsymbol{V}_k = \boldsymbol{J}_{k+1}(R_k)\boldsymbol{V}_{k+1} \tag{2}$$

where R_k is the radius of layer k, $\boldsymbol{V}_k$ is a vector of constants (undetermined coefficients) used to express the displacement solution field for a given mode of deformation. The form of the solutions and the required number of constants are known from Hashin and Rosen [5] or Christensen and Lo [4]. From Eq. (2) one can then derive the solution vector $\boldsymbol{V}_{k+1}$ by defining a transfer matrix $\boldsymbol{N}^{(k)} = \boldsymbol{J}_{k+1}^{-1}(R_k)\boldsymbol{J}_k(R_k)$

$$\boldsymbol{V}_{k+1} = \prod_{j=k}^{1} \boldsymbol{N}^{(j)}\, \boldsymbol{V}_1 \tag{3}$$

Based on this, the average stress and strain in the whole n-layered inclusion can be calculated from the continuity conditions used for the respective modulus, by setting the appropriate components of $\boldsymbol{V}_1$ and $\boldsymbol{V}_{k+1}$ to zero to avoid a singularity at the fiber axis and a divergence at infinity.

In order to determine the effective elastic moduli, the n-layered inclusion is surrounded by an (n+1)-phase which is assumed to have the yet unknown properties of an equivalent homogeneous medium. Uniform strain or stress is applied to the medium at infinity. The effective moduli are obtained by requiring the average strain or stress in the n-phase cylinder to equal the strain or stress of the effective medium at infinity, which is shown to be equivalent to the Christensen-Lo energy condition.

For all but the transverse shear modulus, the effective elastic moduli are directly derived through the recursive algorithm. The solution is found by coincide of upper and lower bounds, as described by Hashin and Rosen [5]. The remaining modulus is determined using a self-consistency condition.

The analytical expressions derived by Hervé and Zaoui can be applied to viscoelastic composites by replacing the elastic phase moduli by the corresponding complex moduli.

The first goal of this work is to evaluate the accuracy of this micromechanical model by comparing the predictions with the finite element estimates described in Section 2.2.

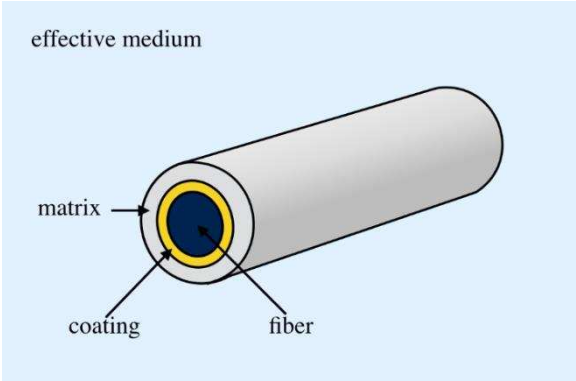

Figure 3: The n-layered model of Hervé and Zaoui for multiple layers of coated fiber-reinforced composites.

3 Theoretical predictions for the viscoelastic properties

3.1 Effect of coating thickness

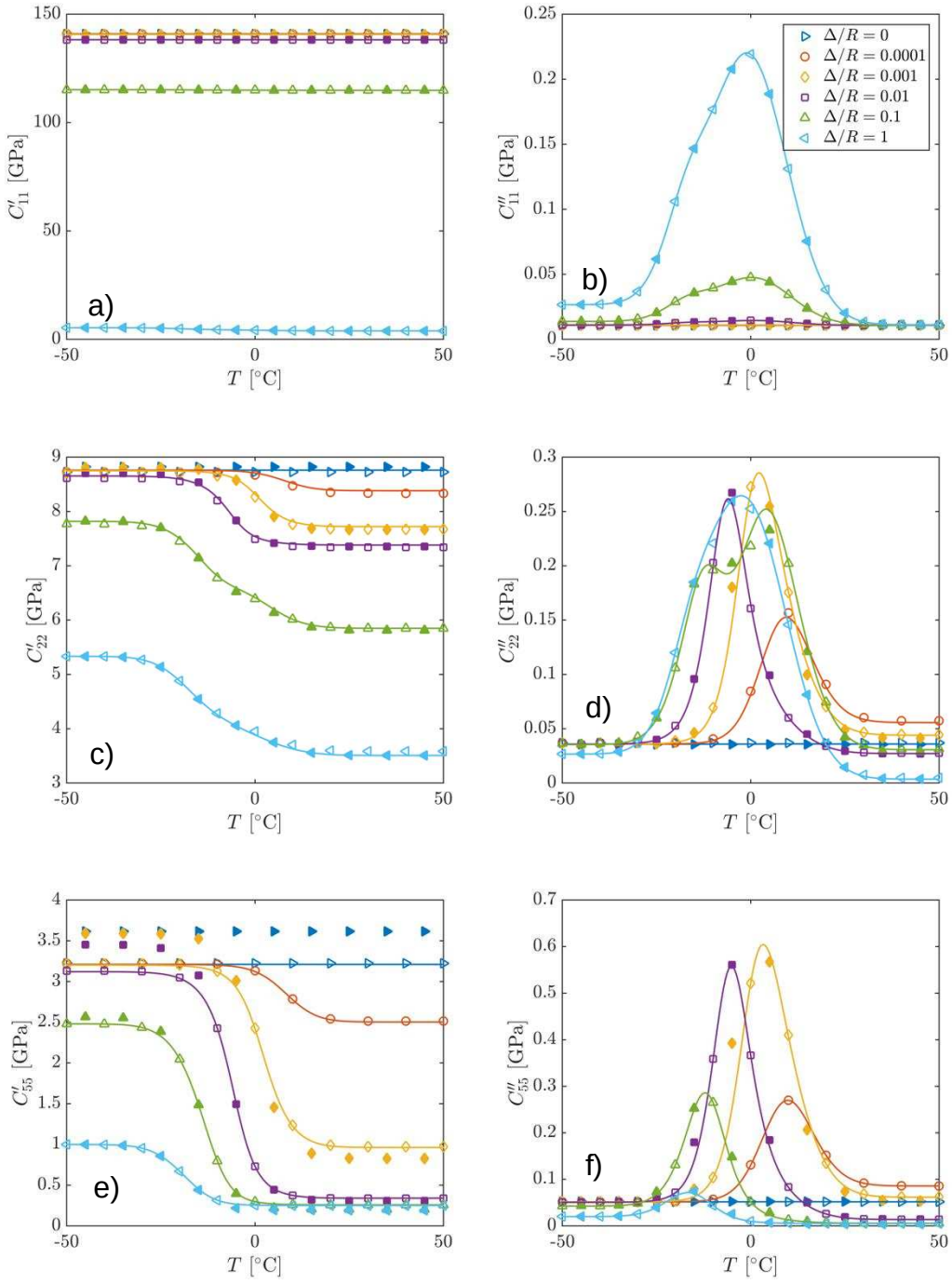

Figure 4: Temperature dependence of the effective viscoelastic moduli for composites with different fiber coating thickness ratios, comparing the n-phase model predictions (lines) with hexagonal (open symbols) and random (closed symbols) finite element models. The coating thickness ratio is indicated by colors where dark blue corresponds to uncoated fibers and light blue to fibers consisting of the coating material only. For the thinnest coating thickness (0.0001), only hexagonal finite element models could be employed with our current computational resources while calculations with the random models were numerically impractical because of too many finite elements required.

The impact of a coating layer was analyzed by comparing three of the five independent moduli which are C_{11}, C_{22} and C_{55}, given in the complex form C_{ik}= C'_{ik}+iC''_{ik}. The predictions of the n-phase model, indicated by lines, are compared to frequency-domain finite element (FE) estimates of hexagonal models (open symbols) and random models (solid symbols). A composite with a fiber volume fraction $\nu_f = 0.6$ was assumed, where the volume fraction is defined as the ratio of the fiber volume, including coating, to the total volume of the unit cell. The moduli for thickness ratios Δ/R = 0.0001, 0.001, 0.01 and 0.1 are shown, where Δ is the thickness of the coating layer and R the outer radius of the fiber together with coating. Using this definition, Δ/R = 0 and Δ/R = 1 then correspond to uncoated carbon fibers and fibers consisting of the coating material only, respectively.

Clearly, the latter results in a strong reduction of the storage modulus C'_{11}, while the loss modulus C''_{11} is overall increased with thicker coating layers as shown in Figure 4a and b, respectively. The estimates of both, the hexagonal and random models, are in equally good agreement with the predictions of the n-phase model for all coating thickness ratios. For the longitudinal direction, a ratio of 0.01 could be viewed as optimum, with an already noticeable increase in C''_{11} for only a small drop in C'_{11}.

The effect of the coating layer thickness is different for the transverse modulus C_{22}. Here, at Δ/R = 1 the storage modulus is only reduced by a factor two at T=50°C compared to uncoated carbon fibers. The loss modulus C''_{22} does not increase continuously for thicker coating layers but shows to reach almost the same peak values for all composites with $\Delta/R \geq 0.001$. With respect to the uncoated fiber composite, it is about seven times larger at the maximum which is reached with a coating thickness ratio of 0.001. However, a small shift of the temperature of maximal loss modulus is observed for different coating thickness ratios. At this point, it is highly remarkable that even for the thin coating thickness ratios, the model predictions and the finite element estimates of the hexagonal model coincide for all temperatures. Some deviations

are however seen with respect to the random models as for C'_{55}. The differences increase the less coating material is used. It is further seen from Figure 4e that the reduction across T_g is higher, compared to the previous discussed moduli. Comparing the loss modulus C''_{55} to C''_{22} for the different coating thicknesses one can see the differences for coating thickness ratios of 0.1 and above. There, the peak values are much smaller than all others. However, for smaller ratios, the behavior for C''_{22} and C''_{55} is similar. The overall maximum for both C''_{22} and C''_{55} is found with $\Delta/R = 0.001$ and is slightly above T_g. For the transverse and shear moduli, a ratio of 0.001 could be viewed as an excellent compromise, with a significant increase in C''_{22} and C''_{55} for only a small drop in both storage moduli compared to uncoated fibers. Additionally, at this coating thickness, Figures 4a and 4b suggest that neither the longitudinal storage or loss moduli would be significantly affected, which could be an important result.

3.2 Effect of fiber volume fraction

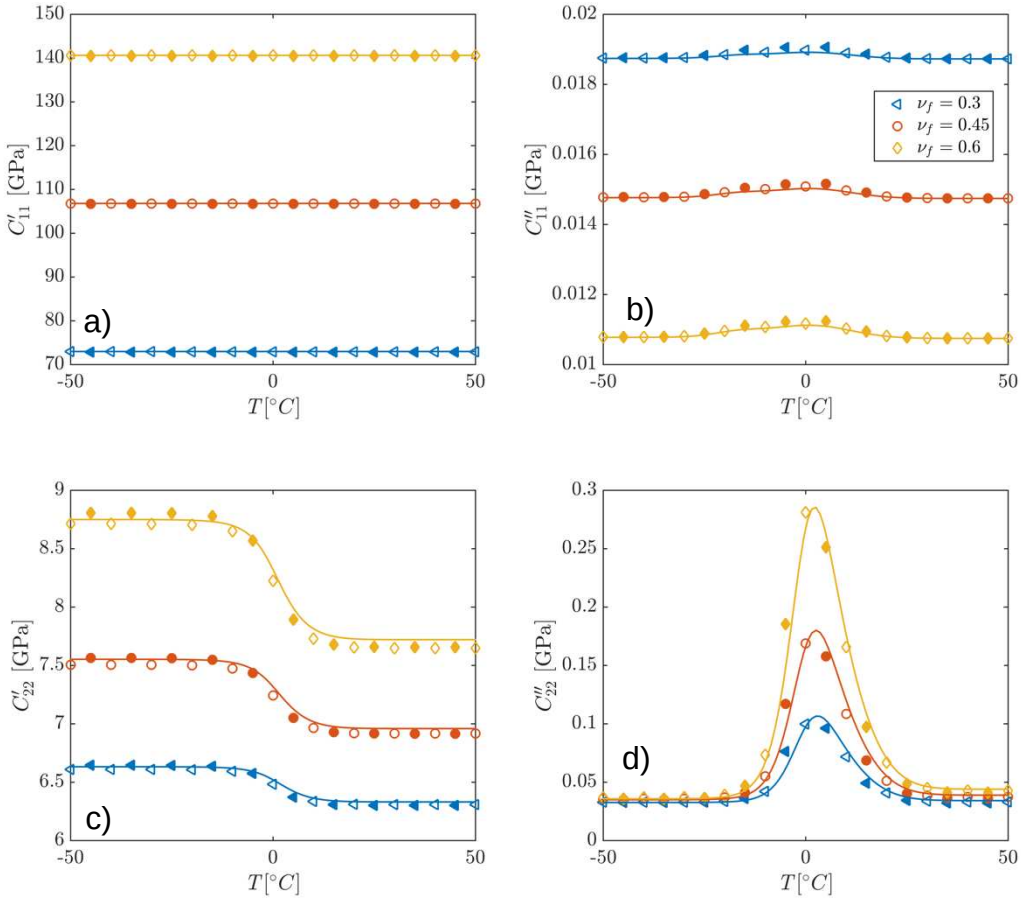

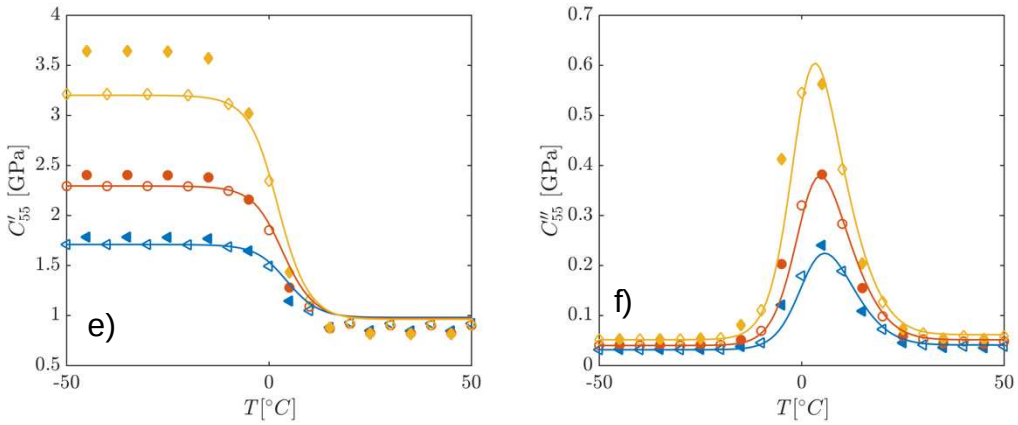

Figure 5: Temperature dependence of C_{11}, C_{22} and C_{55} in terms of storage and loss moduli, C'_{ik} and C''_{ik}, respectively. The effective moduli for three different volume fractions are shown for v_f=0.3 (blue), 0.45 (red) and 0.6 (yellow). Lines indicate the predictions of the n-phase model, symbols correspond to finite element estimates with hexagonal structures (open) and random structures (closed).

Figure 5 demonstrates the temperature dependence for three moduli C_{11}, C_{22} and C_{55}. The results for three different volume fractions v_f are shown, with v_f = 0.3, 0.45 and 0.6. A coating thickness ratio Δ/R = 0.001 was assumed based on the results in Section 3.1.

From Figure 5a, one can clearly see an increase in the stiffness with a higher fiber volume fraction. Raising the volume fraction by a factor of two leads to an increase of C'_{11} by almost the same factor. Only a slight variation with the temperature is seen in both, the storage and the loss moduli. It is further shown that C''_{11} is larger the smaller the volume fraction.

Comparing the model predictions and the FE estimates, the agreement for C_{11} is again excellent. The deviations in the real part are too small to be determined from this figure. For the imaginary parts, slight differences below 1% are seen for the random models around T_g.

Figure 5c and d present the corresponding results of the transverse modulus, C_{22}. In this case, both the storage and the loss modulus are noticeably affected by the temperature and the volume fraction of fibers (which also increases the fraction of the viscoelastic coating). Interestingly, the pattern of behavior, with increasing fiber volume fraction, is different to that seen for C'_{11} and C''_{11}. For the longitudinal constants, as the fiber volume fraction was increased, C'_{11} was

seen to rise (Figure 5a), while C''_{11} fell (Figure 5b). However, for the transverse properties, the pattern was more interesting, and reflects our previously published work on spherical coated particle composites [15]. Here, both C'_{22} and C''_{22} increased with increasing fiber content, with the influence being particularly large for the highest volume fraction of v_f = 0.6.

In contrast to C''_{11}, the loss modulus C''_{22} shows to have a high but narrow peak which is seven times larger (for v_f = 0.6) than at the two terminal temperatures. At the latter, C''_{22} converges to the same value for the three volume fractions, while the peak values deviate. It is further seen, that the peak is located somewhat below the T_g of the coating material.

Although differences between the two finite element models can be seen, the deviations are small (below 2%). The estimates of the hexagonal model are slightly lower than the model predictions, whereas the random model predicts too high moduli.

Interestingly, the agreement of the loss moduli is even more remarkable. Even at T_g where the moduli change rapidly with the temperature, the model predictions are close to the FE estimates. Somewhat larger deviations were however found for C'_{55} below the glass transition temperature, as presented in Figures 5e and f. At v_f = 0.6 the predictions of the random FE models were about 15% too high. However, excellent predictions were still obtained with the hexagonal models. We have already seen such similar behavior in our previous work [21] on unidirectional composites with uncoated glass and carbon fibers. It is a bit surprising that the microstructural effects are the strongest for the C'_{55} axial shear modulus but we cannot offer any immediate explanation to this fact.

3.3 Effect of volume fraction at a fixed temperature of 0°C

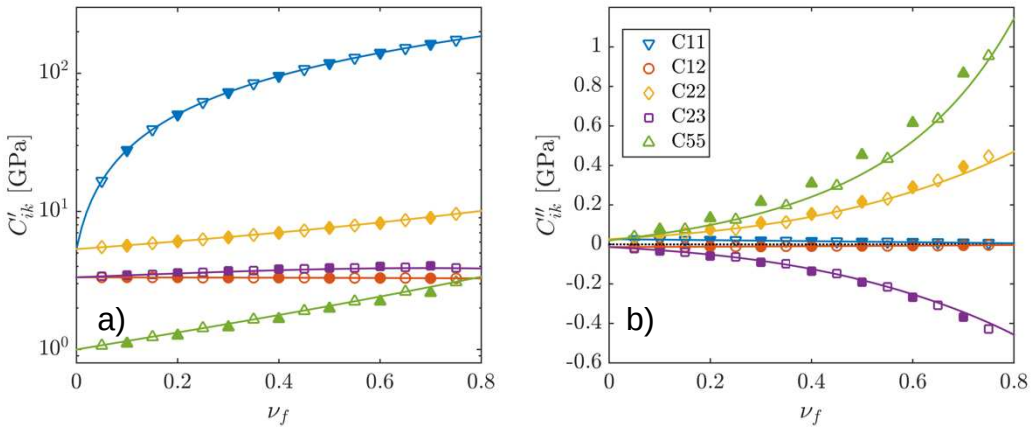

Figure 6: Effective moduli predicted by the n-phase model (lines) and the finite element models with hexagonal structure (open symbols) and random structure (closed symbols). Storage (a) and loss moduli (b) are shown with respect to the fiber volume fraction.

Figure 6 presents the model predictions (lines) and FE estimates (symbols) for the five independent effective viscoelastic coefficients assuming a coating thickness ratio Δ/R= 0.001, so now including the real and imaginary parts of C_{12} and C_{23}. Both hexagonal and random models are used in the FE simulations as indicated by open and solid symbols, respectively. The results are compared for different volume fractions. A constant temperature of 0°C is assumed.

Complementary to the results presented in a previous work [21], it is shown that all storage moduli except C'_{12} increase with the volume fraction ν_f. The loss moduli, on the other hand, decrease with ν_f for C''_{23} and C''_{11}. Further, it is seen that the C''_{23} and C''_{12} have negative values, although C''_{12} is broadly independent of volume fraction.

The storage moduli obtained from the n-phase model are in excellent agreement with the FE predictions, for both the hexagonal and the random model. The agreement is equally good for all coefficients but C'_{55} for which the random model estimates deviate by up to 7%. This difference is also seen in the loss modulus C''_{55} where the deviance is even larger (around 15%).

However, comparing the other loss moduli shows that the three methods give practically indistinguishable results for volume fractions below 0.5. Above this level, small deviations are revealed as both FE models give slightly different results to the n-phase model. This is highlighted in particular by C_{22} and C_{23} where differences of almost 10% are seen.

Similar results were obtained at T=-50°C and T=50°C.

Altogether, it was shown that the n-phase model is suitable to predict the effective viscoelastic moduli of unidirectional fiber reinforced composites. A remarkably high accuracy was seen for both the storage and the loss moduli and the validity was confirmed for various coating layer thicknesses and volume fractions. This confirmation then allows the whole design space to be quickly evaluated, and also will allow aspects such as the properties of an alternative viscoelastic coating to be quickly assessed.

4 Finite element predictions for the plate eigenfrequency spectrum

The previously derived effective viscoelastic moduli of unidirectional coated carbon fiber composites were used to study the eigenfrequencies of a plate strip with those effective properties. A simply supported strip of length L=20cm and thickness H=2mm was considered. The effective moduli were taken from the model predictions for a composite with fiber volume fraction 0.6 and the previously determined optimal coating thickness ratio 0.001. Complex eigenfrequency $f = f' + if''$ and damping time $\tau = 1/f''$ were derived from both plane-strain 2D and 3D finite element simulations.

The equations of motion are given by

$$\rho \frac{\partial^2 \boldsymbol{u}}{\partial t^2} = \nabla \cdot \boldsymbol{\sigma} \tag{4}$$

where $\boldsymbol{u} = \boldsymbol{u}(\boldsymbol{r}, t)$ is the displacement vector at position $\boldsymbol{r}$ at time t, $\nabla \cdot$ the spatial divergence operator and $\boldsymbol{\sigma}$ the instantaneous stress tensor. Here and below, a direct notation is used for the tensors.

A steady-state harmonic form solution

$$\boldsymbol{u}(\boldsymbol{r},t) = \bar{\boldsymbol{u}}(\boldsymbol{r})e^{i\omega t} \tag{5}$$

is assumed, where $\bar{\boldsymbol{u}}$ is the position-dependent complex amplitude of displacement and ω the angular frequency of oscillation.

The strain tensor is defined by

$$\boldsymbol{\varepsilon} = [\nabla\mathbf{u} + (\nabla\mathbf{u})^{\mathrm{T}}]/2 = \bar{\boldsymbol{\varepsilon}}e^{i\omega t} \tag{6}$$

where $\bar{\boldsymbol{\varepsilon}} = \bar{\boldsymbol{\varepsilon}}(\boldsymbol{r})$ is the position-dependent complex strain amplitude tensor. Linear viscoelastic frequency-independent stress-strain constituent relations are assumed

$$\boldsymbol{\sigma} = \boldsymbol{C}\boldsymbol{\varepsilon} = (\boldsymbol{C}' + i\boldsymbol{C}'')\bar{\boldsymbol{\varepsilon}}e^{i\omega t} \tag{7}$$

where $\boldsymbol{C}$ is the viscoelastic complex modulus tensor, $\boldsymbol{C}'$ and $\boldsymbol{C}''$ are the storage and loss moduli, which are given by the real and imaginary parts of the modulus tensor, respectively. The inclusion of frequency dependence does not present any undue complications but it is not needed for the model problems considered in this work.

The discrete dynamic finite element stiffness relations are obtained by substituting Eqs. (5) – (7) in Eq. (4) and using standard Bubnov-Galerkin weak form procedure [23] to get the following matrix differential equation

$$\boldsymbol{M}\ddot{\boldsymbol{a}} + \boldsymbol{C}\dot{\boldsymbol{a}} + \boldsymbol{K}\boldsymbol{a} = \boldsymbol{0} \tag{8}$$

where $\boldsymbol{M}$, $\boldsymbol{C}$ and $\boldsymbol{K}$ are the mass, damping and stiffness matrices, $\boldsymbol{a}$ is a global vector listing the unknown components of the displacement vectors at the nodal points of the studied model and the overdot denotes the derivative with respect to time.

Substituting harmonic form $\boldsymbol{a} = \bar{\boldsymbol{a}}e^{i\omega t}$ in Eq. (8), one obtains the following viscoelastic characteristic value problem

$$\lambda^2\boldsymbol{M}\bar{\boldsymbol{a}} - \lambda\boldsymbol{C}\bar{\boldsymbol{a}} + \boldsymbol{K}\bar{\boldsymbol{a}} = \boldsymbol{0} \tag{9}$$

where $\bar{\boldsymbol{a}}$ denotes the nodal displacement amplitude vector and $\lambda = -i\omega$ the eigenvalue.

Weak-form boundary conditions are imposed using the Lagrange multiplier method. In this study, simply supported boundary conditions are assumed. The resulting sparse-matrix eigenvalue problem is solved using the ARPACK Arnoldi package (www.caam.rice.edu/software/ARPACK) as implemented in COMSOL Multiphysics [20]. The fundamental frequency of a simply supported strip with properties as named above was studied in both plane-strain 2D and 3D FEM simulations.

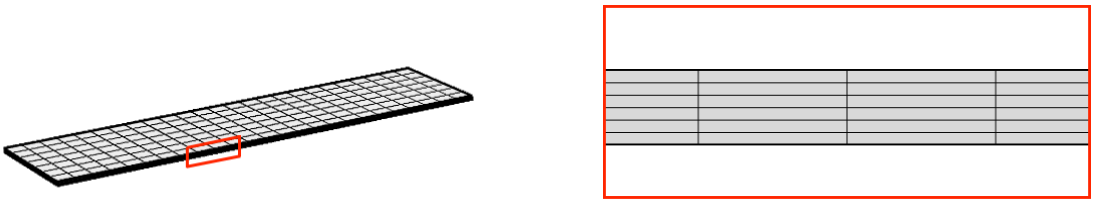

a) b)

Figure 7: Mesh of a 3D finite element model of a strip (a) and magnified view of the highlighted cross section (b) as also used for the plane-strain 2D models.

The 3D model was meshed employing brick elements as depicted in Figure 7a. The largest structure was composed of 30,000 mesh elements. A similar mesh was used for the 2D model by referring to a cross section of the 3D mesh (Figure 7a). Here, the mesh was constituted of 600 rectangular elements. While the calculation time of 2D simulations was only about a second, 3D simulations required up to several minutes.

In the theoretical analysis of elastic plates, one commonly assumes the orthotropic symmetry [24]. Unidirectional composites with perfectly aligned fibers have a fiber symmetry, which is a subset of the more general orthorhombic symmetry class. In the finite element analysis, the required viscoelastic moduli are given by the corresponding viscoelastic moduli tensor represented by standard 6x6 Voigt-notation complex-valued matrices. They involve five independent viscoelastic moduli that are obtained using the n-layered micromechanical models (see Section 3). Two different unidirectional fiber layouts are considered, the one with the fibers along the strip axis (termed longitudinal) and perpendicular to it (termed transverse).

Aiming at comparing derived fundamental frequencies of 2D and 3D models, a parameter study was performed varying the width W of the strip in the 3D model. In this way, both beam-like and plate-like setups could be addressed.

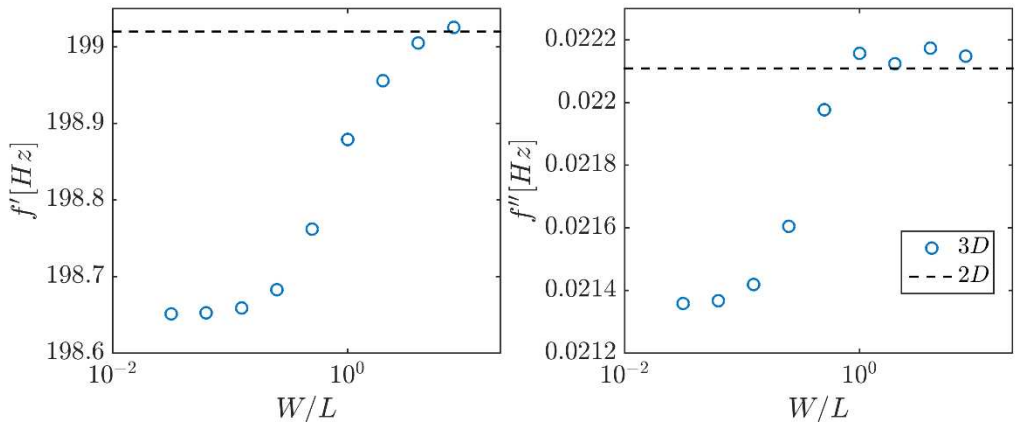

Figure 8: Fundamental frequency $f = f' + if''$ obtained from 2D and 3D finite element simulations. Fibers were assumed to be oriented in the longitudinal direction. The development of the eigenfrequency with different aspect ratios W/L is shown.

Figure 8 shows the fundamental frequency $f = f' + if''$ resulting from these simulations. A clear trend of the eigenfrequency obtained from 3D simulations is seen. When changing from low to high aspect ratios, both the real and the imaginary parts increase. With higher aspect ratio, the eigenfrequencies from 3D models converge towards those from 2D simulations. Some minor differences (below 1%) are found in the imaginary part.

Overall, also the magnitude of increase from low to high aspect ratios is small, i.e. below 1% in the real part and 3% in the imaginary parts.

For the following FEM estimates, 2D simulations were performed as it was shown that comparable results to the 3D model FEM estimates were obtained, but in considerably less computing time.

4.1 Temperature dependence

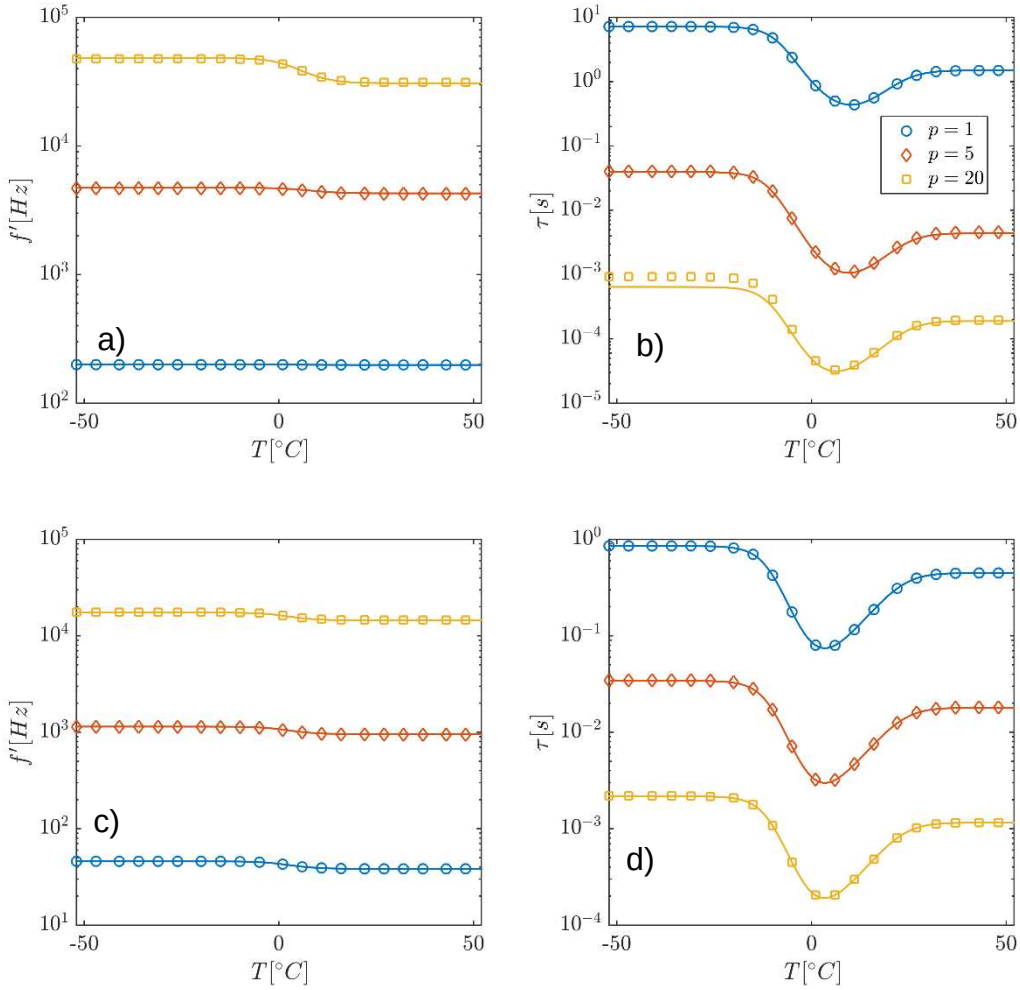

Figure 9: Eigenfrequency f' (left) and damping time $\tau = 1/f''$ (right) of a simply-supported plate strip with fibers oriented in the longitudinal direction (Figures a and b) or the transverse direction (Figures c and d). The temperature dependence is shown for three eigenmodes, p=1, 5 and 20. Micromechanical FEM estimates (symbols) and analytical n-layered model predictions (lines) are used as input for the structural eigenfrequency FEM calculations. A coating thickness ratio of 0.001 is assumed.

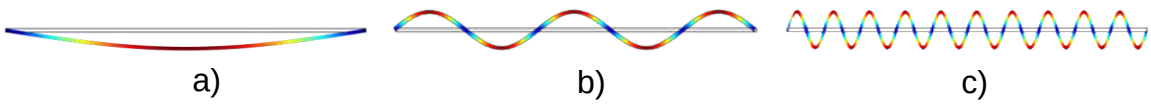

Figure 10: Illustration of the deflection of three studied eigenmodes p=1 (a), 5 (b) and 20 (c).

Figure 9 shows the change of the eigenfrequency and the damping time with temperature for the unidirectional composites with coated carbon fibers assumed to be oriented in the

longitudinal (Figures a and b) or the transverse direction (Figures c and d). Three modes are analyzed with mode numbers p = 1, 5 and 20 as illustrated in Figure 10. Comparing their frequencies in the case of longitudinal oriented fibers, it reveals that the change across T_g is larger for higher modes, whereas the frequency of the fundamental mode remains almost unchanged. Unlike the frequency, the damping time varies also for lower modes. A similar development is found for all three modes. The damping time at the glass transition temperature is reduced by more than one order of magnitude compared to T=-50°C. Also, and significantly, the damping time is still considerably reduced above the glass transition temperature of the coating.

Overall, it is seen, that the higher modes decay faster. For example, the damping time at 50°C of the fundamental mode is about one second, while for p=20 it is less than a microsecond. Similar trends are observed for composites with fibers oriented in the lateral direction.

At this point, it should be mentioned that the eigenfrequencies were calculated assuming frequency-independent properties of the coating material although this does not represent well the real viscoelastic behavior where a frequency change of one order of magnitude corresponds to a temperature shift of 4°C. As shown in Figure 9, an increase in the temperature causes a decrease in the frequency. Hence, also the coating properties will be affected. However, for the fundamental mode, whose decay is commonly most important in structural vibration damping applications, the frequency change is small (below 1%) and therefore the frequency-dependence is expected to have only minor contribution. Frequency-independent moduli are assumed for all further simulations.

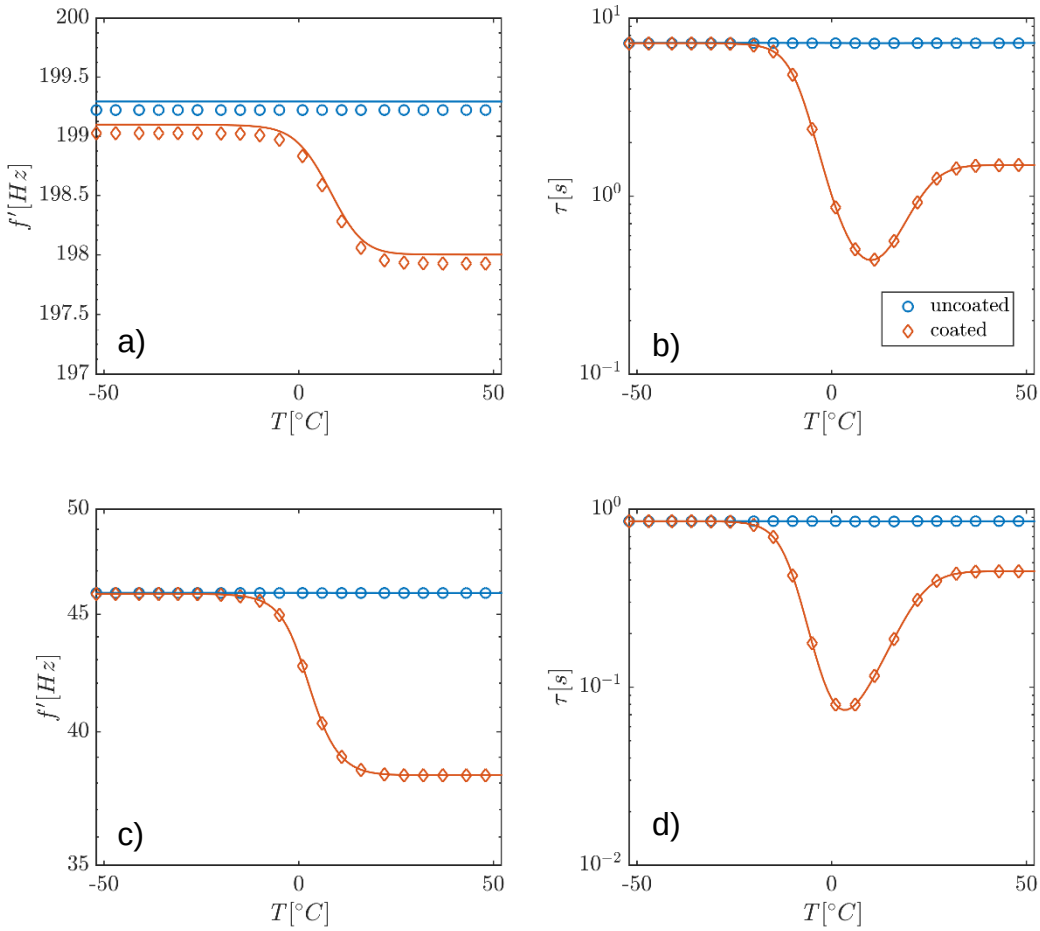

Figure 11: Comparison of the eigenfrequency (left) and damping time (right) of the fundamental mode of a plate strip of uncoated (blue) and coated fiber composite (red) with coating thickness ratio 0.001 for temperatures across T_g. For Figures a and b, longitudinally oriented fibers were assumed whereas for Figures c and d transversely oriented fibers. FEM estimates and analytical predictions are shown as indicated by symbols and lines, respecitvely, as described in the legend to Figure 9.

In the previous figures, only coated fiber composites were considered. However, the influence of the coating layer on plate strip eigenfrequency has not been shown yet. Therefore, frequency and damping time of the fundamental mode are compared in Figure 11 for an uncoated fiber composite and a composite containing coated fibers of coating thickness ratio 0.001. The decrease in the frequency from below to above the glass transition temperature is approximately 0.5% for the coated fiber composite with longitudinal oriented fibers. Considering uncoated fibers, the composite moduli, and hence the frequency, are temperature-independent. The overall effect of the coating layer on the frequency is small as the difference for the two composites is only below 1%.

However, with fibers in the lateral direction, the reduction of the frequency for coated fiber composites is more than 15%.

In both cases, the significance of a coating layer is clearly demonstrated for the damping time. With longitudinally oriented fibers, the minimal damping time of the coated fiber composite is 0.44s which is only 6% of the one obtained for the uncoated fiber composite at the same temperature. With further increase of the temperature the damping time is increased again and converges to 1.5s which is still by factor 5 smaller than with uncoated fibers. Using transversely oriented fibers, this difference is only 50%. At first sight, the results presented in Figure 11b are unexpected, as the previous results from Figures 4b and 5b showed that the longitudinal loss modulus was little affected at this coating thickness ratio. This conflicting result will be explained in the following section.

4.2 Comparison of Classical Plate Theory and First-order Shear Deformation Theory

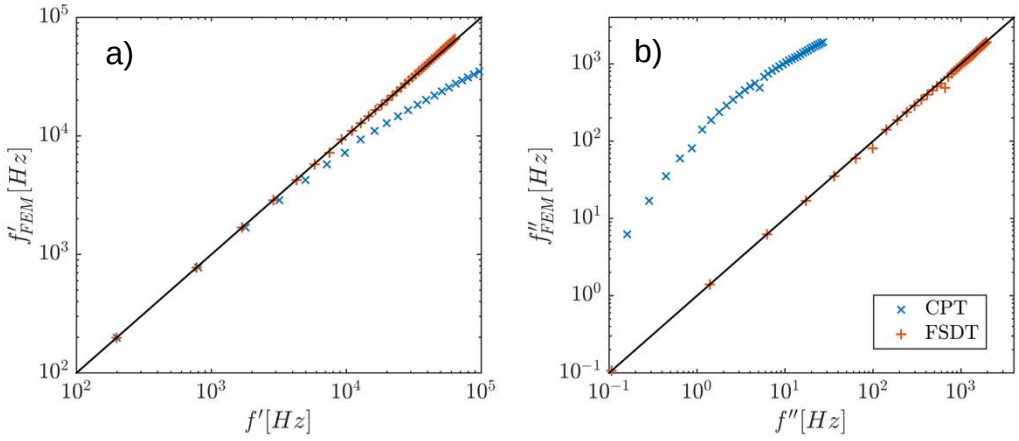

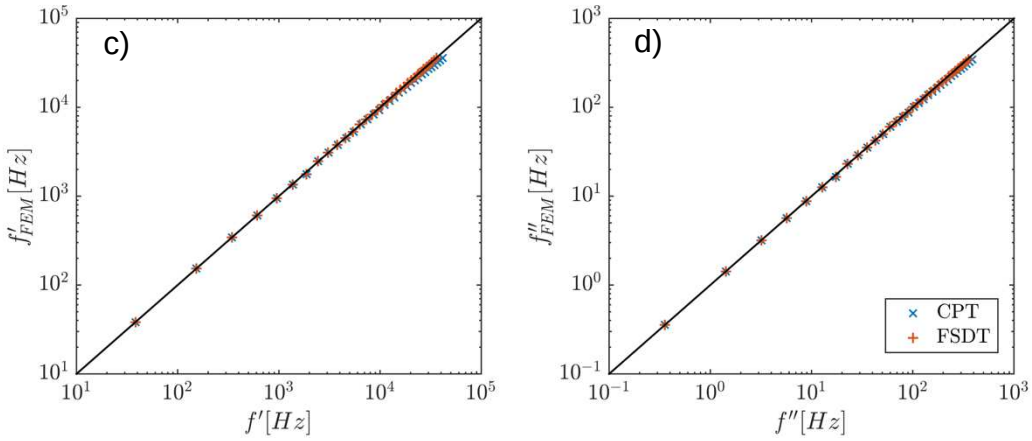

Figure 12: Eigenfrequencies for different modes. Finite element estimates are compared with Classical Plate Theory (blue) and First-order Shear Deformation Theory (red). The fibers were assumed to be oriented in the longitudinal direction (Figures a and b) or the transverse direction (Figures c and d).

Figure 12 compares the eigenfrequencies obtained from two-dimensional FE simulations with the corresponding analytical solutions of Classical Plate Theory (CPT) and First-Order Shear Deformation Theory (FSDT).

The eigenfrequencies in CPT and FSDT are obtained from the harmonic solution of the equation of motion, assuming that the displacements w are of the form

$$w(x,t) = w_0(x)e^{i\omega t} \tag{10}$$

where w_0 is the displacement amplitude and ω the frequency [24]. The eigenfrequencies of mode n are then given by

$$\omega_n^{CPT} = \frac{1}{2\sqrt{3}}\frac{n^2\pi^2}{L^2}H\sqrt{\frac{Q_{11}}{\rho}} \tag{11}$$

in Classical Plate Theory and

$$\omega_n^{FSDT} = \frac{1}{2\sqrt{3}}\frac{n^2\pi^2}{L^2}H\sqrt{\frac{Q_{11}}{\rho}}\sqrt{\frac{1}{1+\frac{1}{K_s}\frac{\pi^2H^2n^2}{L^2}\frac{Q_{11}}{12G_{13}}}} \tag{12}$$

with First-order Shear Deformation Theory, for a strip of length L and thickness H. K_s is the shear correction coefficient and was assumed as $K_s \approx 5/6$. Q_{11} and G_{13} are the plane stress-

reduced longitudinal stiffness and the transverse shear modulus, respectively, and were taken in complex form from the results of Chapter 3.

A volume fraction of 0.6 was assumed and a coating thickness ratio of 0.001. A fixed temperature of 50°C was chosen to achieve frequency-independent properties. For Figure 12a and b, the fibers were considered to be oriented in the longitudinal direction of the strip while for Figure 12c and d fibers in the transverse direction were assumed. The smallest eigenfrequency corresponds to the fundamental mode.

With fibers longitudinally oriented, the discrepancy of the CPT solution is striking. Only the real part of the fundamental mode coincides with the FE solution. For all higher modes, the solutions deviate progressively strongly. Even larger differences are found for the imaginary part, where already the fundamental mode differs by orders of magnitude. The CPT is hence not sufficient to predict complex-valued eigenfrequencies of the composite strip studied.

However, when taking shear effects into account using FSDT, the results agree with the FEM estimates equally good for all modes. Similar results are found for a strip with transverse fibers where FSDT gives reliable predictions for both the real and the imaginary parts. Moreover, also the predictions from CPT are comparable in this case, as the difference to the FE predictions is much smaller than for the previous case of longitudinally oriented fibers. Only small differences in the eigenfrequencies obtained from the two theories can be observed for high modes.

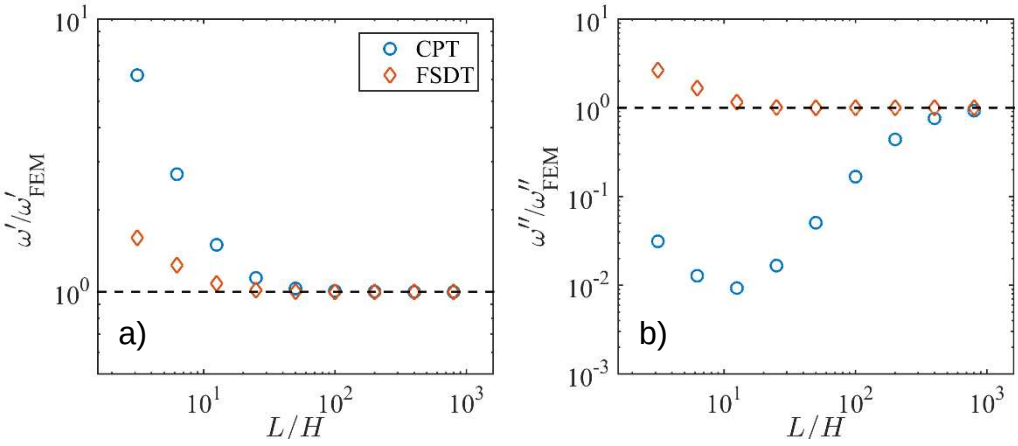

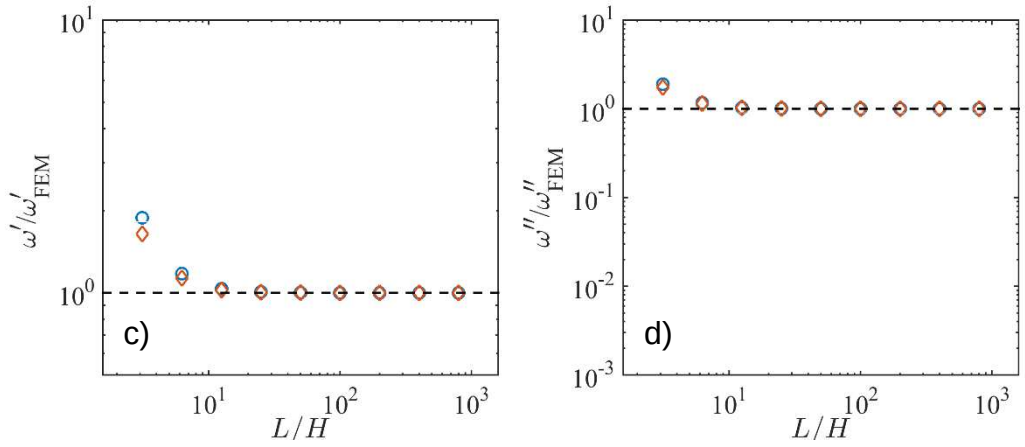

Figure 13: Classical Plate Theory and First-order Shear Deformation Theory predictions for the fundamental frequency with respect to finite element estimates. The convergence with the aspect ratio is shown for a strip with fibers assumed to be oriented in the longitudinal (Figures a and b) or the transverse (Figures c and d) direction.

The difference between Classical Plate Theory and First-Order Shear Deformation Theory was studied in detail for the fundamental mode of a strip with fibers oriented in the longitudinal direction. Figure 13 demonstrates the convergence of the two theories with respect to finite element predictions. The aspect ratio L/H was varied to study the range of validity of the two theories. Considering a strip with fibers oriented in the longitudinal direction, the results obtained from FSDT converge clearly faster than with CPT (Figure a and b). For the real part of the frequency, an aspect ratio of 100 is needed to obtain comparable results from CPT to the FE estimates. With FSDT, the same results can already be achieved for a much smaller aspect ratio. Even larger are the differences in the imaginary part where CPT requires an aspect ratio of almost 1000 to obtain similar results as from FSDT with an aspect ratio of 20.

However, as observed in previous figures, this difference is minor for the transverse case, which suggests that the shear term has no effect here.

Overall, Figure 12 and Figure 13 reveal the differences between CPT and FSDT. It was shown that the validity of CPT is limited to strips with very high aspect ratios. In contrast, FSDT can be widely used and is suitable for the prediction of complex-valued eigenfrequencies. Accurate

estimates are obtained for both the real and imaginary parts and cover lower and higher modes equally good.

These results can then explain the conflicting results from Figures 4b, 5b and 11b. For a highly anisotropic plate, bending in the longitudinal direction excites shear deformation (which has to be taken into account to accurately predict the deformation behavior). Consequently, this excitation of shear deformation in bending also excites enhanced damping behavior.

5 Conclusions

In this work, we presented frequency-domain finite element estimates for unidirectional fiber composites with viscoelastic coating. Finite element models with hexagonal and random microstructures were used and compared to predictions of the n-layered model by Hervé and Zaoui to assess the potential of this model. It was shown for carbon fiber composites that accurate results are obtained. Excellent agreement was found for loss moduli with both, hexagonal and random structure finite element models. While also the predictions of the storage moduli coincided with estimates for hexagonal microstructures, deviations were seen with respect to random microstructures, in particular in the longitudinal shear modulus. However, for the remaining moduli the predictions of the n-layered model were remarkably accurate.

The model is convenient to be applied in micromechanical design to determine optimal properties for coated fiber composites. The present study compared the effective moduli for different coating thicknesses. A maximum in the loss modulus was obtained with coating thickness ratios between 0.01 and 0.001, which corresponds to a coating thickness of 10nm - 100nm [22]. A value of 0.001 was considered optimum, as this gave significant enhancement of the transverse and shear loss moduli, without affecting the longitudinal moduli.

Industrial unidirectional composites commonly have a random microstructure with a variety of local fiber arrangements, as illustrated in Figure 1c. However, classical micromechanical models usually assume a specific, simplified one-fiber arrangement, as illustrated in Figure 3.

It has been shown in both our current and also previous finite element studies [12-14, 21] that despite such simplification, these classical models do provide accurate estimates of the effective viscoelastic elastic moduli and as so, they are very suited for quick and reliable materials design [15, 16, 25]. However, by their construction these models cannot provide detailed information about the distribution of stress fields and their localization in random composites. On contrary, the finite element method directly provides access to such information that can be helpful in studying and understanding both large strain deformation and failure behavior of real composite materials.

In our recent work on coated sphere reinforced composites, we have first demonstrated numerically, using a combination of micromechanical n-layered sphere model's predictions and time-domain finite element estimates, that the loss magnification should occur at a coating thickness ratio of $\Delta/R \sim 0.01$ [12]. And we have then realized this effect experimentally following two different technological routes, by using spray-coated spherical particles [15] and then uncoated ones but dispersed in a phase-separating block-copolymer blend matrix [16, 25]. It will be interesting to see if either of these two manufacturing routes could also be used to experimentally realize the predicted loss magnification effect in unidirectional composites.

Free vibrations of a plate strip were studied as an example of an application to demonstrate the reduction of the damping time through the use of a viscoelastic coating layer. It was shown that for bending in the longitudinal direction, the highly anisotropic nature of the composite (and the high ratio of the longitudinal to the shear moduli) activated significant enhancement of the damping time for this deformation mode due to increased shear deformation.

References

[1] Treviso A, Van Genechten B, Mundo D, Tournour M. Damping in composite materials: Properties and models. Composites Part B: Engineering. 2015;78:144-52.
[2] Ward IM, Sweeney J. Mechanical properties of solid polymers: John Wiley & Sons, 2012.
[3] Christensen RM. Mechanics of composite materials: Courier Corporation, 2012.
[4] Christensen R, Lo K. Solutions for effective shear properties in three phase sphere and cylinder models. Journal of the Mechanics and Physics of Solids. 1979;27:315-30.
[5] Hashin Z, Rosen BW. The elastic moduli of fiber-reinforced materials. Journal of applied mechanics. 1964;31:223-32.
[6] Hervé E, Zaoui A. Elastic behaviour of multiply coated fibre-reinforced composites. International Journal of Enginieering Science. 1995;33:1419-33.
[7] Hill R. Elastic properties of reinforced solids: Some theoretical principles. Journal of the Mechanics and Physics of Solids. 1963;11:357-72.
[8] Herve E, Zaoui A. N-layered inclusion-based micromechanical modelling. International Journal of Engineering Science. 1993;31:1-10.
[9] Seidel GD, Lagoudas DC. Micromechanical analysis of the effective elastic properties of carbon nanotube reinforced composites. Mechanics of Materials. 2006;38:884-907.
[10] Tsukrov I, Drach B, Gross TS. Effective stiffness and thermal expansion coefficients of unidirectional composites with fibers surrounded by cylindrically orthotropic matrix layers. International Journal of Engineering Science. 2012;58:129-43.
[11] Tucker Iii CL, Liang E. Stiffness predictions for unidirectional short-fiber composites: Review and evaluation. Composites Science and Technology. 1999;59:655-71.
[12] Gusev AA. Optimum microstructural design of coated sphere filled viscoelastic composites for structural noise and vibration damping applications. International Journal of Solids and Structures. 2017;128:1-10.
[13] Gusev AA. Time domain finite element estimates of dynamic stiffness of viscoelastic composites with stiff spherical inclusions. International Journal of Solids and Structures. 2016;88:79-87.
[14] Gusev AA. Finite element estimates of viscoelastic stiffness of short glass fiber reinforced composites. Composite Structures. 2017;171:53-62.
[15] Unwin AP, Hine PJ, Ward IM, Fujita M, Tanaka E, Gusev AA. Escaping the Ashby limit for mechanical damping/stiffness trade-off using a constrained high internal friction interfacial layer. Scientific Reports. 2018;8.
[16] Unwin AP, Hine PJ, Ward IM, Fujita M, Tanaka E, Gusev AA. Novel phase separated multi-phase materials combining high viscoelastic loss and high stiffness. Composites Science and Technology. 2018;167:106–14.
[17] Gusev AA, Hine PJ, Ward IM. Fiber packing and elastic properties of a transversely random unidirectional glass/epoxy composite. Composites Science and Technology. 2000;60:535-41.
[18] Hashin Z. Thermoelastic properties of fiber composites with imperfect interface. Mechanics of Materials. 1990;8:333-48.
[19] Hashin Z. Complex moduli of viscoelastic composites—I. General theory and application to particulate composites. International Journal of Solids and Structures. 1970;6:539-52.
[20] Chen Q, Wang G, Chen X, Geng J. Finite-volume homogenization of elastic/viscoelastic periodic materials. Composite Structures. 2017;182:457-70.
[21] Gusev AA, Kern LS. Frequency-domain finite element estimates of viscoelastic stiffness of unidirectional composites. Composite Structures. 2018;194:445-53.

[22] Soden P, Hinton M, Kaddour A. Lamina properties, lay-up configurations and loading conditions for a range of fibre-reinforced composite laminates. Composites Science and Technology. 1998;58:1011-22.
[23] Zienkiewitz OC, R.L. T. The Finite Element Method. Volume 1: The Basis. 5th ed. Oxford: Butterworth-Heinemann Linacre House, 2000.
[24] Reddy JN. Theory and analysis of elastic plates and shells. 2 ed. Boca Raton, Florida: CRC press, 2006.
[25] Unwin AP, Hine PJ, Ward IM, Guseva OA, Schweizer T, Fujita M, et al. Predicting the visco-elastic properties of polystyrene/SIS composite blends using simple analytical micromechanics models. Composites Science and Technology. 2017;142:302-10.